CARBON 50 (2012) 1338–1345

Available at www.sciencedirect.com

SciVerse ScienceDirect

journal homepage: www.elsevier.com/locate/carbon

Synthesis of reduced graphene oxide–Fe_3O_4 multifunctional freestanding membranes and their temperature dependent electronic transport properties

T.N. Narayanan [a], Zheng Liu [a], P.R. Lakshmy [b], Wei Gao [a], Yutaka Nagaoka [c], D. Sakthi Kumar [c], Jun Lou [a], Robert Vajtai [a], P.M. Ajayan [a,*]

[a] Department of Mechanical Engineering and Materials Science, Rice University, Houston, TX 77005, USA
[b] Department of Metallurgical and Materials Engineering, National Institute of Technology, Tiruchirappalli 620 015, India
[c] Bio-Nano Electronics Research Center, Toyo University, 2100, Kujirai, Kawagoe, Saitama 350 8585, Japan

ARTICLE INFO

Article history:
Received 21 March 2011
Accepted 5 November 2011
Available online 12 November 2011

ABSTRACT

A simple and scalable method for the synthesis of reduced graphene oxide (RGO) based conductive and magnetic multifunctional films (membranes) is reported. A RGO–iron oxide (Fe_3O_4) freestanding film is fabricated using a versatile chemical route followed by vacuum infiltration. Temperature dependent electronic transport properties of the magnetic GO and RGO films were measured using a four probe technique from room temperature to 15 K. A conduction mechanism based on variable range hopping is suggested for explaining of the electronic conductivity variations. Possible applications of this multifunctional membrane are also discussed.

1. Introduction

Recent advances in graphene research [1–5] have opened new avenues for fabricating various multifunctional membranes suitable for use in various applications. Out of various graphitic materials, graphene oxide (GO) represents an excellent system, due to the availability of various functional groups, for the synthesis of hybrid materials via wet chemical routes [6–8]. The most versatile and extendable approach for the exfoliation of graphite is by complete oxidation to oxidized graphitic single layers called GO [9]. These hydrophilic, insulating GO can be reduced to conductive reduced graphene oxide (RGO, chemically modified graphene sheets) by various methods [10] and they can find numerous applications in a range of various electronic and display devices [11].

Synthesis of hybrid materials with magnetic and graphitic nanostructures is highly demanding due to their extensive applications in various fields such as catalysis, water purification, sensors, capacitors and bio-medical diagnosis and therapy [6,7]. Recently, graphene based magnetic structures are receiving interest from research community due to their planar geometry and interesting carrier transport properties [12]. Among various magnetic materials, iron oxide (Fe_3O_4/γFe_2O_3) possesses a unique position due to its considerably high saturation magnetization (87 emu/g), interesting electronic transport properties [13] and above all high bio-compatibility [14]. Superparamagnetic iron oxide nanoparticles (SPIONs) based aqueous ferrofluids (FF) were already proven for their application in magnetic hyperthermia (using their radio frequency power loss), magnetic contrast enhancement [15], enzyme immobilization of cell targeting, drug targeting and delivery [16]. The hybrid structures with iron oxide and conductive graphene sheets can find innumerable applications ranging from electromagnetic shielding to medical therapy and treatment [17]. Moreover, these hybrid structures may also exhibit interesting magneto resistance (MR) properties [12].

* *Corresponding author:* Fax: +1 713 348 5423.
E-mail address: ajayan@rice.edu (P.M. Ajayan).
0008-6223/$ - see front matter
doi:10.1016/j.carbon.2011.11.005

Metal–insulator transition in magnetite (Fe_3O_4) known as Verwey transition is one of the important phase transitions that fascinated generations of physicists [18]. Electron–phonon interactions have been attributed to the driving force for this phase transition and this mechanism is interpreted as charge ordering or charge-orbital ordering in literature, though a lot of conflicts still exist on this regard [18]. Electronic transport studies of correlated Fe_3O_4 nanoparticles with weakly correlated systems such as graphene will help to get deeper insights to the nature of electron–lattice coupling and studies on these aspects are seldom seen in literatures. Very recently, couple of authors reported the synthesis of covalently functionalized GO suspensions with magnetic materials [6,7]. Though they could synthesize functionalized GO with ferrocene/iron oxide, extent of magnetic functionalization and phase purity of the particles are still in question [7]. In the present investigation, RGO–Fe_3O_4 conductive and magnetic freestanding films (membranes) are fabricated for the first time, to the best of our knowledge, using a versatile chemical co-precipitation route followed by vacuum infiltration and reduction using hydrazine monohydrate. The electronic transport properties of GO as well as RGO–Fe_3O_4 membranes were studied using a four probe technique in a series of temperatures.

Fe_3O_4, possessing inverse spinel cubic structure, is an attractive catalyst for many applications and interactions between water and iron oxide have been studied by number of researchers in the recent past [19–21]. Ultraviolet photoelectron studies conducted on Fe_3O_4 by Joseph et al. [20] indicates that its surface mainly contains three types of species namely; hydrogen bonded condensed ice, physisorbed water and chemisorbed water. Recently, Chenggang et al. [21] conducted a theoretical study on the dissociative chemisorption of water on the surface of Fe_3O_4 and it indicates that it is essential to understand the mechanism so that Fe_3O_4 will be a useful material for many other adsorption phenomena like water gas shift reaction to produce hydrogen gas. Moreover, Fe_3O_4 are useful for photocatalytic splitting of water and graphitic-Fe_3O_4 conductive heterogeneous membranes are ideal templates for such studies. Fe_3O_4 nanoparticles are well known for their application in water treatment [22], by magnetic separation, adsorption and complexation. The removal of hazardous particles from solution by employing magnetic field is more selective, efficient and faster than other conventional techniques such as centrifugation or filtration [22]. However, an appropriate membrane is required to efficiently use these nanoparticles for water treatment. Here we report on our work to fabricate and test conductive RGO–Fe_3O_4 membranes for the ion adsorption efficiency in salinated water and the initial results are presented in the paper.

2. Experimental methods

2.1. Synthesis of GO suspension

Exfoliated GO suspension has been prepared by the modified Hummer's method [23]. The detailed process is as follows: graphitic powder (Bay carbon Inc., SP-1 grade 325 mesh) was added to the hot (80 °C) mixture of conc. H_2SO_4 (50 ml), $K_2S_2O_8$ (10 g), and P_2O_5 (10 g) with prolonged magnetic stirring. This mixture is diluted using deionized water (DI) ~2 l and vacuum infiltrated through a Teflon filter paper of pore radius 0.1 μm. The filtrate is dispersed in conc. H_2SO_4 (0.5 l) using extensive magnetic stirring and keeping the temperature less than 10 °C using an ice bath. Fifty grams of $KMnO_4$ is added to this solution keeping the temperature at ~10 °C. To this dispersion ~1 l DI water is added by controlling the temperature not to exceed 50 °C. Again ~3 l DI water is added within a time period of 2 h with constant stirring. After 2 h, 50 ml of 30% H_2O_2 is added to this dispersion and this yellowish dispersion is aged for 2 days. This dispersion is again filtered using 0.1 μm Teflon filter paper and the filtrate is sequentially washed with 10% HCl and ~5 l DI water. The filtrate is dried in air and is dispersed in DI water using a mild sonication. The resulting GO suspension seemed to be stable in water for a longer duration.

2.2. Synthesis of magnetic GO suspension

Uniformly sized Fe_3O_4 nanoparticles were synthesized within the GO suspension using a chemical co-precipitation technique. One milliliter of 0.1 M $FeSO_4{\cdot}7H_2O$ and 1 ml of 0.2 M $FeCl_3$ were taken in a conical flask and mixed well using sonication. One milliliter of this solution was added to 10 ml of GO suspension and magnetically stirred for half an hour. Ammonia solution was dropped into this mixture until the pH of the solution reached 10 while constantly stirring it. As soon as the pH reached 10, 3 M citric acid solution is added drop wise and heated the solution to 75 °C, keeping a constant magnetic stirring for 30 min. This solution was filtered (100 nm Teflon filter paper) and the material on the filter set up was let dry over night. The freestanding GO–Fe_3O_4 layer was peeled out from the filter paper and soaked in 2 M hydrazine monohydrate (in 20 ml DI water) and annealed at 90 °C for 1 h. The resultant chemically modified membrane labeled RGO–Fe_3O_4.

The structural and morphological analysis of RGO–Fe_3O_4 membrane were carried out using high resolution transmission electron microscopy (HRTEM, JEM 2100F TEM), field emission scanning electron microscopy (SEM, JEOL 6500F) and atomic force microscopy (AFM, digital instrument nanoscope IIIA). Raman studies were conducted on both GO–Fe_3O_4 and RGO–Fe_3O_4 using a micro-Raman spectroscope (Renishaw, inVia). The reduced and unmodified membranes were analyzed using X-ray photoelectron spectroscopy (XPS, PHI Quantera XPS) and fine analysis was carried out to find out the oxidation state of iron (Fe) in the different samples. The Fourier transform infrared spectroscopy (FTIR) studies on the sample are conducted using a Nicolet FTIR microscope. The DC electrical measurements are carried out in a CTI Cryogenics system, which is connected with a Keithley 2400 source meter to perform current–voltage (*I–V*) test. The magnetization measurements on membrane samples are conducted using a Vibrating Sample Magnetometer (EG&G Par 4500).

3. Results and discussion

A schematic of a single layer of the prepared RGO–Fe_3O_4 membrane is shown in Fig. 1 (the basal plane (gray in color)

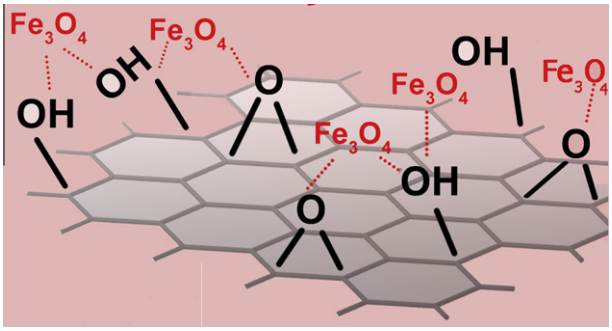

Fig. 1 – Schematic of single layer of RGO–Fe_3O_4 multifunctional membrane. The red dotted line indicates the covalent interaction of oxygen functionalities in RGO with citric acid coated Fe_3O_4 (red) nanoparticles. (For interpretation of the references to color in this figure legend, the reader is referred to the web version of this article.)

is the RGO membrane). Fig. 1 shows the interaction of Fe_3O_4 nanoparticles with RGO membrane via covalent interactions (dotted red lines). The surface coated Fe_3O_4 nanoparticles using citric acid interact with oxygen functionalities of GO. This covalent bond remains stable even after hydrazine hydrate reduction to form RGO–Fe_3O_4. This covalent interaction has been further proved by FT-IR analysis.

The cross-sectional SEM of RGO–Fe_3O_4 membrane is shown in Fig. 2(a). The thickness of the film seems to be ~10 μm. Fig. 2(b) depicts the HRTEM image of the membrane after dispersing the membrane in acetone by extensive sonication and drop casting this solution in a holey carbon coated copper grid. The graphitic planes are visible and are marked. The contrast portions in HRTEM indicated the magnetic nanoparticles and the planes have been identified as that of iron oxide.

The iron oxide nanoparticles are seen dispersed uniformly in the membrane with an average particle size around 11 nm. The selected area electron diffraction (SAED) shown in Fig. 2((b), inset) indicates the presence of amorphous RGO and nano-crystalline iron oxide in the membrane.

AFM has been used to characterize the surface structure of the hybrid RGO–Fe_3O_4 films in the tapping mode (Fig. 2(c) and (d)). The AFM images, especially, the phase image (Fig. 2(d)), clearly indicate that the iron oxide nanoparticles are imbedded inside the RGO matrix uniformly. The phase imaging seems very capable of characterizing such combined structure due to the various mechanical properties between RGO and iron oxide nanoparticles. According to the cross-section analysis for typical areas, the diameter of iron oxide particles ranges from 10 to 15 nm, which is well in agreement with the HRTEM results.

Raman spectroscopic studies on GO as well as RGO iron oxide membrane were conducted using the 514.5 nm laser.

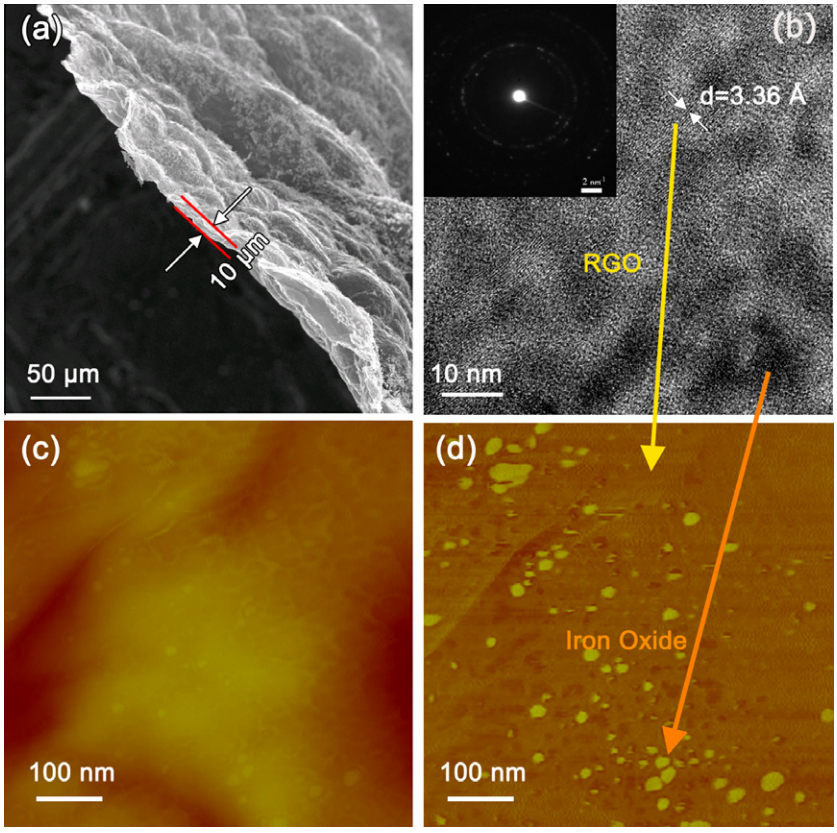

Fig. 2 – (a) Cross-sectional SEM image of RGO–Fe_3O_4 freestanding membrane. The white arrows with red parallel lines indicate the thickness of the film (~10 μm). (b) HRTEM image of RGO–Fe_3O_4. The dark contrast indicates the magnetic Fe_3O_4 nanoparticles. The (1 1 1) crystal plane of Fe_3O_4 having lattice spacing, d = 3.36 Å is identified in the figure. Inset shows the SAED of RGO–Fe_3O_4. (c) and (d) AFM images of RGO–Fe_3O_4 freestanding membrane. (For interpretation of the references to color in this figure legend, the reader is referred to the web version of this article.)

Fig. 3 shows the Raman results before and after reduction. The graphitic D and G peaks are clearly seen and I_G/I_D intensity ratio seems to have decreased after reduction, indicating the decrease in the average size of sp^2 domain upon reduction of the exfoliated GO and it is well acknowledged by the researchers [10].

XPS analysis was conducted to identify the extent of reduction and types of ions present in the membrane. Moreover, it

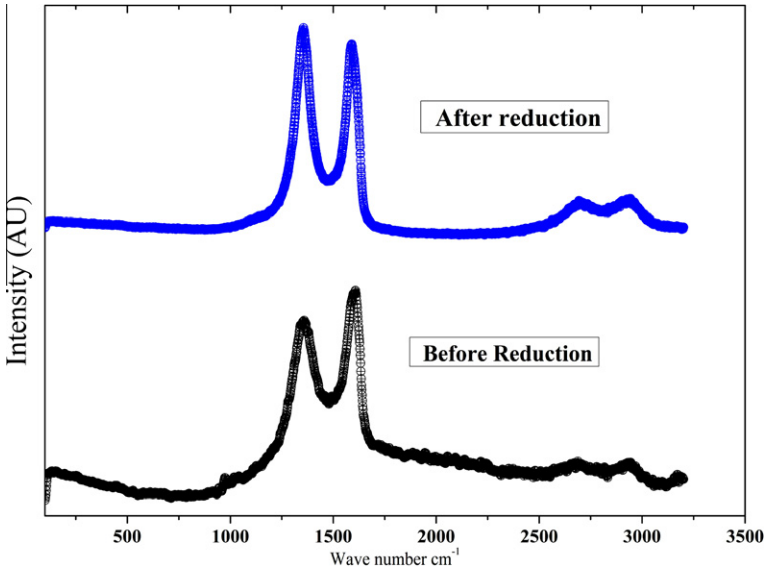

Fig. 3 – Micro-Raman spectra of GO/iron oxide (black) and RGO/iron oxide (blue). (For interpretation of the references to color in this figure legend, the reader is referred to the web version of this article.)

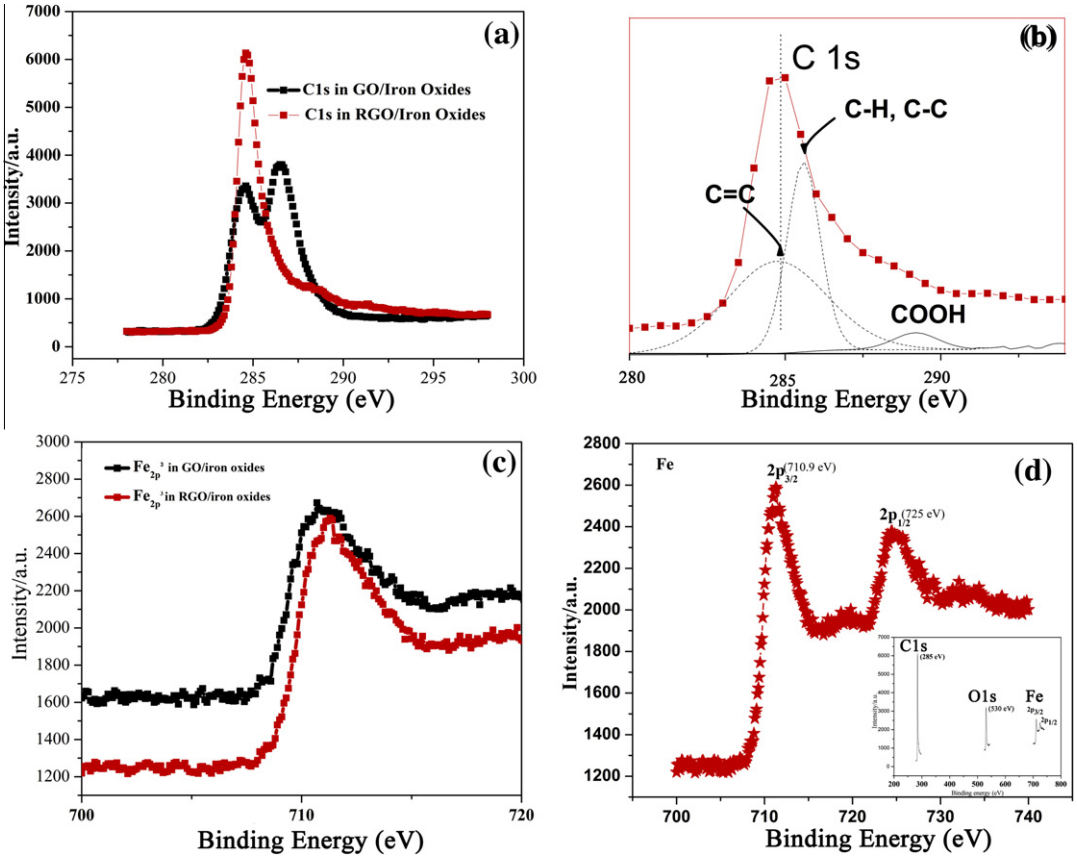

Fig. 4 – XPS of GO/iron oxide (black) and RGO/iron oxide (red); (a) C 1s, (b) C 1s of RGO/iron oxide with deconvolution fittings, (c) and (d) Fe 2p. (For interpretation of the references to color in this figure legend, the reader is referred to the web version of this article.)

also helps to identify the oxidation state of iron oxide (it is hard to distinguish Fe_3O_4 from γFe_2O_3 using a simple XRD analysis [24]).

XPS spectra indicate the presence of three elements, carbon (C 1s at 285 eV), oxygen (O 1s at 530 eV) and iron (Fe 2p at 710 eV) (Fig. 3(c) inset). The detailed deconvolution of XPS spectra has been carried out using multipack software and it is plotted in Fig. 4(a)–(c). The deconvoluted C 1s spectrum implies that, GO–Fe_3O_4 consists of functional groups such as sp^2 (C= C, 284.8 eV), epoxy/hydroxiyls (C–O, 286.2 eV), Carbonyl (C=O, 287.8 eV) and carboxylates (O–C=O, 289 eV) [9]. The deconvolution of C 1s indicates that (Fig. 4(b)) RGO–Fe_3O_4 consists a main peak centered at 284.8 eV (carbon sp^2), representing the reduction of GO into RGO after the chemical treatment using hydrazine monohydrate. Smaller shoulder peaks corresponding to COOH and C–H functionalities also exist. This is also in tune with the earlier reports that –COOH groups are unlikely to be completely reduced by low temperature hydrazine monohydrate reduction [25]. The percentage of reduction of GO has been evaluated using carbon/oxygen ratio (C/O) from XPS analysis. GO–Fe_3O_4 possesses C and O abundances of 70% and 30%, respectively. It is seen that the C/O ratio is ~15 for the RGO–Fe_3O_4, indicating the reduction of functional groups. A detailed analysis on Fe 2p spectrum indicates that the iron oxide present is Fe_3O_4. The peaks of Fe $2p_{1/2}$ and Fe $2p_{3/2}$ at 710.9 eV and 725 eV establish the fact that the iron oxide in the sample is Fe_3O_4 [26].

The FT-IR analysis of the samples shows the chemical bonding information in GO, GO–Fe_3O_4 and RGO–Fe_3O_4 (Fig. 5).

The presence of different types of oxygen functionalities in GO, such as oxygen stretching vibration (2900–3600 cm^{-1}, –OH vibration), C=O stretching (1720 cm^{-1}), C–OH stretching vibration (1220 cm^{-1}), and C–O stretching vibration (1060 cm^{-1}) is evident from Fig. 5(a). Moreover, signature of aromatic C=C stretching at ~1600 cm^{-1} indicates the presence of sp^2 hybridized honeycomb lattice. The GO–Fe_3O_4 also contains these functional groups, but the positions of the bonds are red shifted and sharpness of the peaks are changed, particularly that of aromatic C=C bonding. This indicates the change in the coordination environment of various functional groups in GO–Fe_3O_4. The peaks between 400 and 700 cm^{-1} are corresponding to that of Fe–O in Fe_3O_4. The shift in the peak position and modification of C=C bonding is proposed as the evidence for covalent bonding in GO [27]. The absorbance intensity of various functional groups in RGO–Fe_3O_4 is reduced compared to GO–Fe_3O_4 indicating the reduction of GO. However presence of unreduced functional groups in RGO–Fe_3O_4 is clear and is supporting the XPS results.

3.1. DC conductivity studies

The schematic of the four probe *I–V* measurement is shown in the inset of Fig. 6(a).

A high vacuum of ~10^{-6} Torr and lowest temperature of 15 K can be achieved by this system. The fluctuation of temperature is less than 1% and the current is limited below 1.5 mA to avoid heating effect, ensuring the validity of the data. All *I–V* curves of RGO–Fe_3O_4 membrane exhibit good linear relationship, indicating an Ohmic contact between RGO–Fe_3O_4 film and electrodes (Fig. 6(a)) and metallic like behavior of the RGO–Fe_3O_4 membrane. But the room temperature *I–V* curve of GO–Fe_3O_4 is not a linear one showing its non-conducting/semiconducting nature and it is depicted in Fig. 6(d). The conductivity versus temperature of RGO–Fe_3O_4 film is shown in Fig. 6(b). In comparison to the electrical conductivity of RGO film by Gómez-Navarro et al. [28], there are two significant improvements in the present case. The reported conductivity of reduced GO lies within the range 10^{-3}–2 S/cm [28,29]. In the present case, RGO–Fe_3O_4 hybrid structure exhibited an increased conductivity. With an annealing temperature as low as 90 °C, the conductivity of RGO–Fe_3O_4 film is comparable with the conductivity values of recently reported reduced graphene oxide annealed under 600 °C [9]. Secondly, the conductance of RGO–Fe_3O_4 film decreases by 11.5% from room temperature to 14.8 K, contrasting sharply with RGO film whose conduction dependence on temperature shows an exponential decrease. Therefore, it is reasonable to believe that the existence of Fe_3O_4 nanoparticles modified the conductance of RGO film, forming a good conducting material that combines the advantages of magnetic nanoparticles and chemically modified graphene layers.

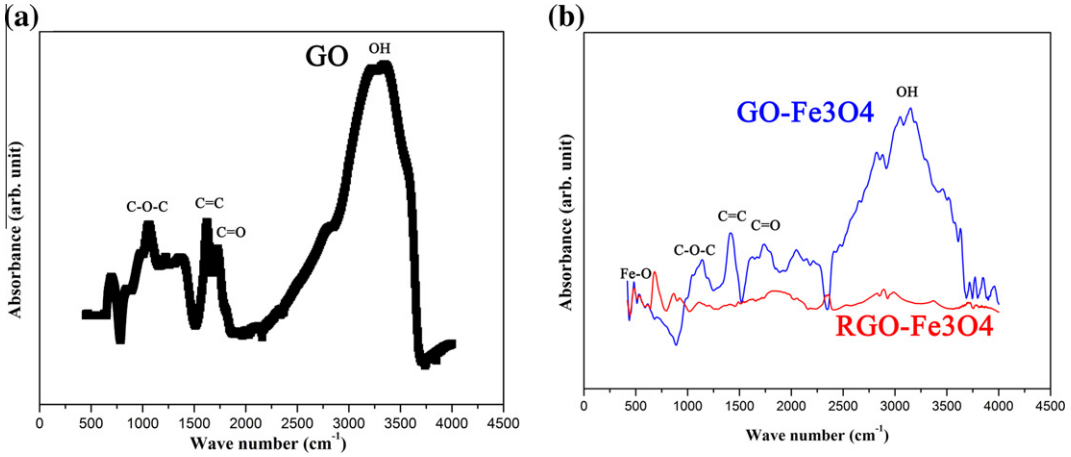

Fig. 5 – FT-IR spectra of (a) GO, (b) GO–Fe_3O_4 (blue) and RGO–Fe_3O_4 (red). (For interpretation of the references to color in this figure legend, the reader is referred to the web version of this article.)

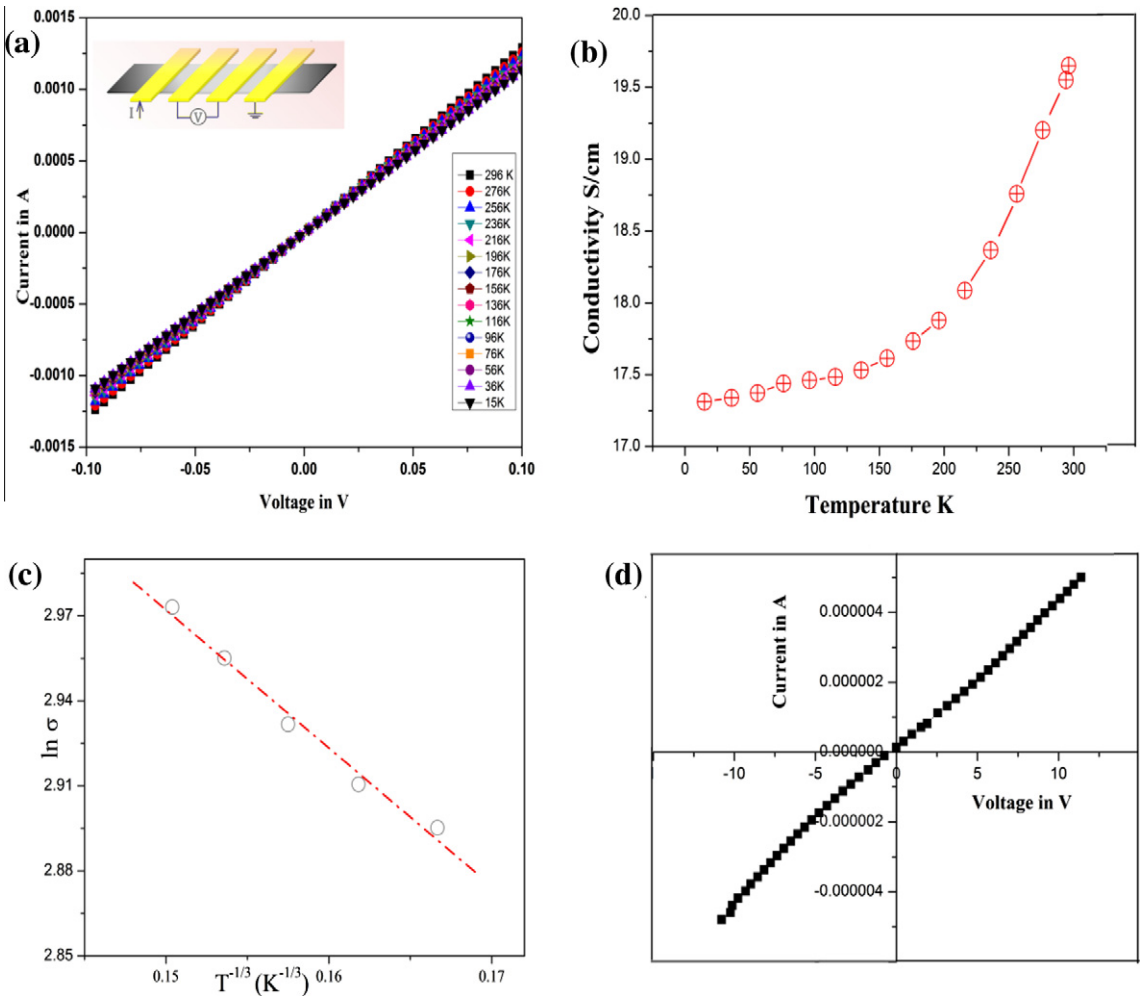

Fig. 6 – (a) *V–I* curves (inset, schematic of four probe *I–V* measurement), (b) temperature–conductivity curve, (c) VRH theoretical fitting ranging from 200 K to 300 K, for RGO–Fe_3O_4 freestanding film; (d) *V–I* curve for GO–Fe_3O_4 freestanding film.

To elucidate the temperature-related conduction mechanism of RGO–Fe_3O_4 film, the variable ranging hopping (VRH) [30–32] of electrons is considered. In the VRH scenario, the hopping probability of electrons in two dimensional system sharply decrease at low temperature, resulting into an exponential reduction of conduction. It has been used to explain the conduction behavior of many two dimensional systems such as amorphous carbon [33], single-wall carbon nanotube networks [34] and reduced GO film [28].

According to the VRH theory, the conductivity and temperature follows the relation:

$$G = G_0 \exp[-(T_0/T)^{\alpha}], \quad (1)$$

where G_0, T_0 are characteristic conductance and temperature of the material, respectively. Exponent α indicates an exponential temperature dependence and can be written as $d + 1$, here d indicates the dimensionality of the system. Fig. 6(c) shows the fitting result for $\ln\sigma$ versus $T^{-1/3}$, which exhibits a good linear relationship ranging from 200 K to 300 K. In the present case, $\alpha = 1/3$ which fits well with the obtained conductivity and it describes a classic two dimensional conducting behavior, reflecting its consistency with the 2D structure of the film. Here, the VRH theory fitting parameter G_0 and T_0 are 40.4 S/cm and 115.4 K, respectively. However, the VRH theory seems to be not applicable below 150 K due to the abnormal conductivity change of Fe_3O_4 (magnetite). While the conductivity decreased quickly from room temperature to 150 K the decrease rate becomes slow when the temperature is below this value, showing a change in the conduction mechanism. The abnormal conduction change of Fe_3O_4 (magnetite), known as Verwey transition (metal–insulator transition), accounts for this change. As Verwey found [35], bulk magnetite undergoes a transition at around 120 K, where a discontinuity in the structure, conductivity and magnetic properties has been observed. Although this effect has been extensively investigated, various explanations have been proposed and it remains highly controversial. The transition temperature in our case is about 150 K, larger than the value of bulk magnetite. We believe the larger surface-to-volume ratio of iron nanoparticles than bulk leads a higher transition temperature, which is consistent with previous report on magnetite nanocrystals and single-crystal thin films [36]. These studies also imply that magnetite nanocrystals are well bonded to the RGO structure forming an ideal composite.

3.2. *Magnetization studies*

Magnetization studies on RGO–Fe_3O_4 membrane have been carried out using VSM in both parallel and perpendicular to the membrane. Both the samples exhibit superparamagnetic behavior as expected for uniformly distributed non-interacting, single domain (since particle size is ~12 nm, it is below the critical particle size) and super paramagnetic Fe_3O_4 particles (Fig. 7) [22]. The small paramagnetic contribution is not subtracted and it may is assumed to be coming from the graphitic membrane.

The perpendicular field measurement exhibited a higher saturating field compared to the parallel field measurement as it is inferred from Fig. 7. This investigation reveals the formation of 'in-plane' linear superparamagnetic Fe_3O_4 nanoparticles chains as it is reported in the case of polymer–Fe_3O_4 nanocomposites [37]. This again validates the layer-by-layer formation of RGO–Fe_3O_4 membrane and uniform distribution of nanoparticles in each membrane.

These magnetic and conductive membranes have innumerable applications in various fields [38,39]. The RGO–Fe_3O_4 membranes were also tested for their efficiency for ion adsorption from salinated water. The results are presented in Fig. 8.

The salinity of the water was measured using a conductivity probe (VWR TRACEABLE) and initial salinity was found to be ~38.1 mS/cm (Galveston water, TX, USA). Even in the absence of any external potential the conductivity seemed to drop constantly, while the RGO–Fe_3O_4 membrane was immersed in saline water (Fig. 8). Fe_3O_4 is a well known adsorbent for heavy metal ions present in sea water [26,37]. This implies that these membranes have potential applications in fields such as water purification. Ashish et al. [26] reported the desalination efficiency of Fe_3O_4 decorated multiwall carbon nanotubes supercapacitors and found 70% sodium removal efficiency. RGO based Fe_3O_4 can possess a much higher efficiency due to its planar structure and enhanced surface of contact. Moreover, it can even work with very highly saline water such as sea water where normal electrodeionization process will not work.

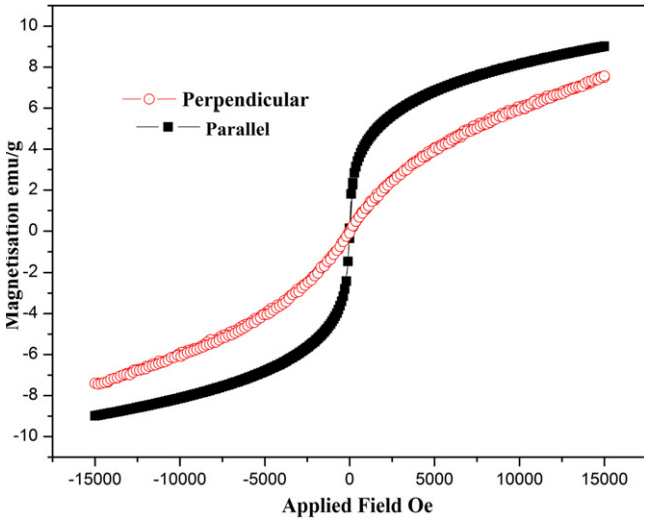

Fig. 7 – Magnetization curve (*M*(*H*) curve) for RGO/iron oxide freestanding film.

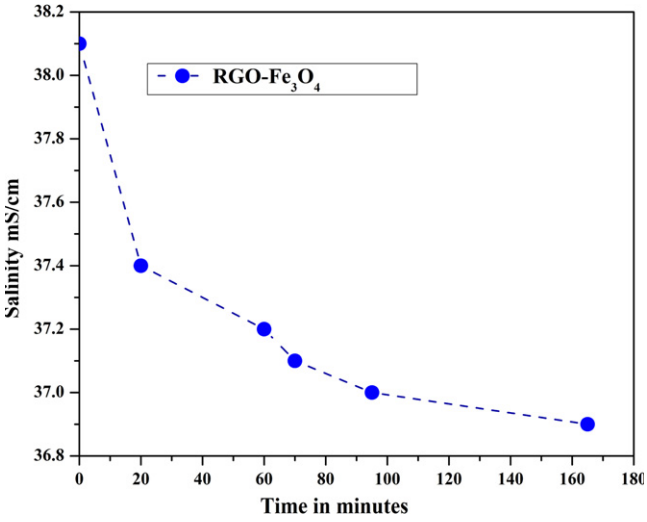

Fig. 8 – Desalination test using RGO–Fe_3O_4 membrane.

4. Summary and outlook

GO and RGO–Fe_3O_4 magnetic freestanding membranes were realized by a novel chemical route followed by vacuum infiltration. The temperature dependent DC conductivity studies on these membranes indicate that both RGO and Fe_3O_4 contribute to the transport phenomena indicating the well physical and chemical binding of the nanoparticles to the graphitic matrix. A VRH conduction mechanism was identified in the case of RGO–Fe_3O_4 membrane in a temperature region of 200–300 K. A drastic change in the mechanism of conduction near 150 K is owed to the Verwey metal–insulator transition of Fe_3O_4. The conductive RGO–Fe_3O_4 is successfully tested for its application in water desalination showing its versatile futuristic potentials. These membranes also find applications in supercapacitors, catalysis, bio-medical fields and electromagnetic radiation shielding devices.

Acknowledgement

The authors gratefully acknowledge the financial support from Nanoholdings LLC, Rowayton, CT.

REFERENCES

[1] Geim AK. Graphene: status and prospects. Science 2009;324:1530–4.
[2] Ci L, Song L, Jin CH, Jariwala D, Wu DX, Li YJ, et al. Nat Mater 2010;9(5):430–5.
[3] Wei L, Dai-Ming T, Yan-Bing H, Con-Hui Y, Zhi-Qiang S, Xue-Cheng C, et al. Low-temperature exfoliated graphenes: vacuum-promoted exfoliation and electrochemical energy storage. ACS Nano 2009;3(11):3730–6.
[4] Rui W, Yufeng H, Ziqian W, Hao G, John TLT. Large diameter graphene nanotubes synthesized using Ni nanowires templates. Nano Lett 2010;10(12):4844–50.

[5] Inhava J, Dmitri AD, Richard DP, Rodney SR. Tunable electrical conductivity of individual graphene oxide sheets reduced at low temperatures. Nano Lett 2008;8(12):4283–7.
[6] Guoxiu W, Bei W, Jinsoo P, Juan Y, Xiaoping S, Jane Y. Synthesis of enhanced hydrophilic and hydrophobic graphene oxide nanosheets by a solvothermal method. Carbon 2009;47:68–72.
[7] Jianfeng S, Yizhe H, Min S, Na L, Hongwei M, Mingxin Y. One step synthesis of graphene oxide-magnetic nanoparticle composite. J Phys Chem C 2010;114:1498–503.
[8] Sheng C, Junwu Z, Xiaodong W, Qiaofeng F, Xin W. ACS nano from graphene to metal oxide nanolamellas: a phenomenon of morphology transmission. ACS Nano 2010;4(10):6212–8.
[9] Daniela CM, Dmititry VK, Jacob MB, Alexander S, Zhengzong S, Alexander S, et al. Improved synthesis of graphene oxide. ACS Nano 2010;4(8):4806–14.
[10] Stankovich S, Dikin DA, Piner RD, Kohlaas KA, Kleinhammes A, Jia Y, et al. Synthesis of graphene based nanosheets via chemical reduction of exfoliated graphite oxide. Carbon 2007;45:1558–65.
[11] Neil RW, Priyanka AP, Richard B, Robert JY, Ian AK, Lei G, et al. Graphene oxide: structural analysis and application as a highly transparent support for electron microscopy. ACS Nano 2009;3(9):2547–56.
[12] Niu ZP, Li FX, Wang BG, Sheng L, Xiang DY. Spin transport in magnetic graphene super lattices. Eur Phys J B 2008;66:245–50.
[13] Hongliang L, Yihong W, Zaibang G, Shijie W, Kie LT, Teodor V. Effect of antiphase boundaries on electrical transport properties of Fe_3O_4 nanostructures. Appl Phys Lett 2005;86:252507-1–3.
[14] Narayanan TN, Reena Mary AP, Anas SPK, Sakthi Kumar D, Makarov D, Albrecht M, et al. Enhanced bio-compatibility of ferrofluids of self-assembled super paramagnetic iron oxide-silica core-shell nanoparticles. J Nanosci Nanotechnol 2011;11:1958–67.
[15] Reena Mary AP, Narayanan TN, Sunny V, Sakthi Kumar D, Yasuhiko Y, Joy PA, et al. Synthesis of bio-compatible SPION based aqueous ferrofluids and evaluation of radio frequency power loss for magnetic hyperthermia. Nanoscale Res Lett 2010;5:1706–11.
[16] Tapan KJ, Marco AM, Sanjeeb KS, Diandra LLP, Vinod L. Iron oxide nanoparticles for sustained delivery of anticancer agents. Mol Pharm 2005;2(3):194–205.
[17] Narayanan TN, Sunny V, Shaijumon MM, Ajayan PM, Anantharaman MR. Enhanced microwave absorption in nickel filled multiwall carbon nanotubes in the S band. ECS Lett 2009;12(4):K21–4.
[18] Shchennikov VV, Ovsyannikov SV. Is the Verwey transition in Fe_3O_4 magnetite driven by a Peierls distortion. J Phys: Condens Matter 2009;21:271001.
[19] Joseph Y, Ranke W, Weiss W. Water on FeO(1 1 1) and Fe_3O_4(1 1 1): adsorption behavior on different surface terminations. J Phys Chem B 2000;104:3224–36.
[20] Joseph Y, Kuhrs C, Ranke W, Weiss W. Adsorption of water on Fe_3O_4(1 1 1) studied by photoelectron and thermal desorption spectroscopy. Surf Sci 1999;433:114–8.
[21] Chenggang Z, Qingfan Z, Lei Z, Bo H, Gang N, Jinping W, et al. Density functional theory study of water dissociative chemisorption on the Fe_3O_4(1 1 1) surface. J Phys Chem C 2010;114:21405–10.
[22] Cafer TY, Mayo JT, William WY, Arjun P, Joshua CF, Sujin Y, et al. Low-field magnetic separation of monodisperse Fe_3O_4 nanocrystals. Science 2006;314:964–7.
[23] Wei G, Lawrence BA, Lijie C, Ajayan PM. New insight in to the structure and reduction of graphite oxide. Nat Chem 2009;1:403–8.
[24] Benjamin G, Jordan EK, Jonathan DD, Yadong Y, Roger F, Glen AW. Soft X-ray spectroscopy study of the electronic structure of oxidized and partially oxidized magnetite nanoparticles. J Phys Chem C 2010;114:21994–2001.
[25] Li D, Müller MB, Gilje S, Kaner RB, Wallace GG. Processable aqueous dispersions of graphene nanosheets. Nat Nanotechnol 2008;3:101–5.
[26] Asish KM, Ramaprabhu S. Magnetite decorated multiwalled carbon nanotube based super capacitor for arsenic removal and desalination of seawater. J Phys Chem C 2010;114:2583–90.
[27] Avinash MB, Subrahmanyam KS, Sundarayya Y, Govindaraju T. Covalent modification and exfoliation of graphene oxide using ferrocene. Nanoscale 2010;2:1762–6.
[28] Gómez-Navarro C, Weitz RT, Bittner AM, Scolari M, Mews A, Burghard M, et al. Electronic transport properties of individual chemically reduced graphene oxide sheets. Nano Lett 2007;7(11):3499–503.
[29] Eda G, Fanchini G, Fanchini M. Large area ultrathin films of reduced graphene oxide as a transparent and flexible electronic material. Nat Nanotechnol 2008;3(5):270–4.
[30] Miller A, Abrahams E. Impurity conduction at low concentrations. Phys Rev 1960;120(3):745–55.
[31] Mott SN. Electrons in glass. Rev Mod Phys 1978;50(2):203–8.
[32] Sheng P. Fluctuation-induced tunneling conduction in disordered materials. Phys Rev B 1980;21(6):2180–95.
[33] Robertson J. Amorphous carbon. Adv Phys 1986;35(4):317–74.
[34] Jaiswal M, Wang W, Fernando KAS, Sun YP, Menon R. Magneto transport in transparent single-wall carbon nanotube networks. Phys Rev B 2007;76(11):113401-1–4.
[35] Verwey EJW, Haayman PW. Electronic conductivity and transition point of magnetite (Fe_3O_4). Physica 1941;8(9):979–87.
[36] Lee S, Fursina A, Mayo JT, Yavuz CT, Colvin VL, Sumesh Sofin RG. Electrically driven phase transition in magnetite nanostructures. Nat Mater 2008;7(2):130–3.
[37] Novakova AA, Smirnov EV, Gendler TS. Magnetic anisotropy in Fe_3O_4–PVA nanocomposites as a result of Fe_3O_4 nanoparticles chains formation. J Magn Magn Mater 2006;300:e354–8.
[38] Kangfu Z, Yihua Z, Xiaoling Y, Chunzhong L. One-pot synthesis of graphene/Fe_3O_4 composites by a solvothermal reaction. New J Chem 2010;34:2950–5.
[39] Jiajie L, Yanfei X, Dong S, Long Z, Yi H, Yanfeng M. J Phys Chem C 2010;114:17465–71.